eNeuro

Research Article: New Research | Sensory and Motor Systems

Odor-induced multi-level inhibitory maps in *Drosophila*

https://doi.org/10.1523/ENEURO.0213-19.2019

Cite as: eNeuro 2019; 10.1523/ENEURO.0213-19.2019

Received: 5 June 2019
Revised: 6 December 2019
Accepted: 16 December 2019

1. Title

Odor-induced multi-level inhibitory maps in *Drosophila*

2. Abbreviated title

Inhibitory odor maps

3. Author names and Affiliation

Veit Grabe[1], Marco Schubert[1,2], Martin Strube-Bloss[1,3], Anja Reinert[1,4], Silke Trautheim[1], Sofia Lavista-Llanos[1], André Fiala[5], Bill S. Hansson[1], and Silke Sachse[1]

[1] *Max Planck Institute for Chemical Ecology, Department of Evolutionary Neuroethology, Hans-Knöll-Str. 8, 07745 Jena, Germany.*

[2] *current address: Freie Universität Berlin, Department of Biology, Chemistry and Pharmacy, Institute of Biology - Neurobiology, Königin-Luise-Strasse 1-3, 14195 Berlin, Germany.*

[3] *current address: Julius-Maximilians-Universität Würzburg, Department of Behavioral Physiology and Sociobiology, Am Hubland, 97074 Würzburg, Germany.*

[4] *current address: Leipzig University, Faculty of Veterinary Medicine, Institute of Anatomy, Histology and Embryology, An den Tierkliniken 43, 04103 Leipzig, Germany.*

[5] *University of Göttingen, Department of Molecular Neurobiology of Behavior, Johann-Friedrich-Blumenbach-Institute for Zoology and Anthropology, Julia-Lermontowa-Weg 3, 37077 Göttingen, Germany.*

4. Corresponding author

Dr. Silke Sachse, Department of Evolutionary Neuroethology, Max Planck Institute for Chemical Ecology, Hans-Knöll-Str. 8, 07745 Jena, Germany.

Tel: +49-3641-571405, Fax: +49-3641-571402, Email: ssachse@ice.mpg.de

5. Number of Figures

7

6. Number of Tables

None

7. Number of Multimedia

None

8. Number of words

Abstract: 158 Introduction: 665 Discussion: 1,992

9. Acknowledgements

We thank Sonja Bisch-Knaden for statistical advice, Mathias Ditzen for programming tools in IDL, Walton Jones and Leslie B. Vosshall for help with generating UAS-Clomeleon flies, Thomas Kuner for helpful advice regarding Clomeleon imaging, Erich Buchner and Thomas Völler for assistance with the initial establishment of chloride imaging, Thomas Kuner, Andreas Schäfer and Marcus Stensmyr for thoughtful comments on the manuscript, and Michelle Wibraham and Andrew Davis for editorial assistance.

S.S. generated transgenic Clomeleon flies and, together with A.F., established initial Clomeleon imaging experiments. V.G., A.R. M.S. and S.T. carried out imaging experiments. M.S.B. helped with data analysis. S.L.L. provided genetic expertise. B.S.H. provided intellectual and financial support. S.S. designed and supervised all experiments. V.G. and S.S. interpreted the results, prepared the figures, and, together with all other authors, wrote the paper.

10. Conflict of Interest

The authors declare no competing financial interests.

11. Funding sources

This work was supported by a BMBF grant to S.S., V.G., M.S.-B., A.R. and S.T., by the Max Planck Society, and by the German Research Foundation (SPP1392 FI-3-1 and SA 909/3-1, 3-2) to A.F. and S.S..

Odor-induced multi-level inhibitory maps in *Drosophila*

Abstract

Optical imaging of intracellular Ca^{2+} influx as a correlate of neuronal excitation represents a standard technique for visualizing spatiotemporal activity of neuronal networks. However, the information-processing properties of single neurons and neuronal circuits likewise involve inhibition of neuronal membrane potential. Here, we report spatially resolved optical imaging of odor-evoked inhibitory patterns in the olfactory circuitry of *Drosophila* using a genetically encoded fluorescent Cl^- sensor. In combination with the excitatory component reflected by intracellular Ca^{2+} dynamics, we present a comprehensive functional map of both odor-evoked neuronal activation and inhibition at different levels of olfactory processing. We demonstrate that odor-evoked inhibition carried by Cl^- influx is present both in sensory neurons and second-order projection neurons, and is characterized by stereotypic, odor-specific patterns. Cl^- mediated inhibition features distinct dynamics in different neuronal populations. Our data support a dual role of inhibitory neurons in the olfactory system: global gain control across the neuronal circuitry and glomerulus-specific inhibition to enhance neuronal information processing.

Significance Statement

Neural inhibition is evidently as important as excitation given it is present at every level of sensory processing. This study characterizes odor-evoked inhibitory patterns along different levels of olfactory processing of *Drosophila* using functional imaging via *Clomeleon*, a genetically encoded indicator for chloride ions, the main mediator of synaptic inhibition in mature neurons. In combination with the excitatory

component reflected by intracellular calcium, we analyzed the interplay between odor-evoked excitation and inhibition. Our data provide both a more accurate and comprehensive characterization of the actual information content encoded by the olfactory circuitry, as well as elucidate network properties within the primary olfactory center of the fly.

Introduction

Inhibition of neural excitability is a ubiquitous feature of all neuronal circuits. Neurons that release inhibitory transmitters are present in all parts of the nervous system. In the olfactory systems of both insects and vertebrates, inhibition is crucial for stimulus gain control (Olsen and Wilson, 2008; Root et al., 2008), synchronizing neural networks (Laurent et al., 2001), generating precise timing (Schoppa and Westbrook, 1999; Margrie and Schaefer, 2003), broadening transmission of olfactory signals (Nagel et al., 2014), odor mixture interactions (Mohamed et al., 2019) and enhancing contrast between similar odor representations (Mori et al., 1999; Sachse and Galizia, 2002; Urban, 2002). In the mammalian olfactory bulb, inhibition is largely mediated by dendrodendritic synaptic connections between excitatory mitral cells and inhibitory granule cells (Schoppa and Urban, 2003; Egger and Urban, 2006). Despite these important roles of inhibition for odor processing, most studies analyzing olfactory coding at the level of spatially distributed neuronal populations focused on monitoring neuronal excitation. Therefore, odor representations at the level of the insect antennal lobe (AL) or the vertebrate olfactory bulb typically have been characterized as patterns of excitation. Here, we aimed at monitoring spatially distributed maps of odor-evoked inhibition at different levels of processing in *Drosophila melanogaster*.

114 In the fly, odors are detected by olfactory sensory neurons (OSNs) located on
115 the antennae and maxillary palps. Each OSN typically expresses one or very few
116 chemo-receptor genes, and each OSN projects its axon to the AL, the insect
117 analogue of the vertebrate olfactory bulb. In the AL, those OSNs expressing the
118 same odorant receptor (OR) stereotypically converge to the same spatially invariant
119 olfactory glomeruli (Couto et al., 2005; Fishilevich and Vosshall, 2005), each of
120 which can be unambiguously identified (Laissue et al., 1999; Grabe et al., 2015). The
121 AL is densely innervated by local interneurons (LNs) that mediate both
122 intraglomerular and transglomerular inhibition (Wilson and Laurent, 2005; Seki et al.,
123 2010). Olfactory projection neurons (PNs) convey the olfactory signals to higher-
124 order brain centers.

125 The morphological structure of the AL network specifies the physiological
126 logic of how odors are encoded: Each odorant evokes a characteristic,
127 spatiotemporal activity pattern leading to a combinatorial, stereotypic activation of
128 glomeruli in the AL (Fiala et al., 2002; Wang et al., 2003). Inhibitory LNs provide both
129 feedforward synaptic inhibition of PNs and feedback inhibition of OSNs (Wilson and
130 Mainen, 2006; Olsen and Wilson, 2008; Root et al., 2008). However, it still remains
131 elusive how spatially distributed, odor-evoked inhibition interferes with and relates to
132 the well-described excitation-based odor maps.

133 In *Drosophila*, functional imaging has mainly relied on genetically expressed
134 Ca^{2+} sensors that detect intracellular Ca^{2+} dynamics as a correlate of neuronal
135 excitation (Grienberger and Konnerth, 2012). In this study, we monitored odor-
136 induced inhibitory maps in the olfactory circuitry using a DNA-encoded indicator for
137 Cl^-, the main ionic mediator of synaptic inhibition in mature neurons (Owens and
138 Kriegstein, 2002). The FRET-based indicator Clomeleon consists of a Cl^--sensitive

139 yellow fluorescent protein (YFP) and a Cl^--insensitive cyan fluorescent protein (CFP)
140 (Kuner and Augustine, 2000). Binding of Cl^- to YFP reduces its absorbance, which
141 results in a change of the YFP/CFP emission ratio proportional to $[Cl^-]_i$. The
142 applicability of Clomeleon *in vivo* has been demonstrated in hippocampal slices
143 (Berglund et al., 2006), retinal bipolar cells (Haverkamp et al., 2005; Duebel et al.,
144 2006), thalamo-cortical neurons of mice (Glykys et al., 2009) and cerebellar granule
145 cells (Berglund et al., 2016).

146 We genetically expressed Clomeleon in defined olfactory neurons and
147 characterized odor-evoked inhibition at different levels of olfactory processing in
148 comparison with Ca^{2+}-mediated activity using the likewise FRET-based Ca^{2+}-
149 sensitive protein Cameleon 2.1 (Miyawaki et al., 1999). First, we observed odor-
150 evoked Cl^--influx in dendrites of OSNs. Second, we generated a comprehensive
151 functional map of both odor-evoked activation and inhibition of the fly AL. We
152 demonstrate that odor-evoked inhibition carried by Cl^- influx is characterized by
153 stereotypic odor-specific patterns. Third, we show that Cl^- mediated inhibition
154 exhibits distinct features at different levels of olfactory processing pointing towards
155 multiple roles of inhibition in the olfactory system.

156

157 **Materials & Methods**

158 **Drosophila stocks and *in vivo* preparation**

159 All fly stocks were maintained on conventional cornmeal-agar-molasses medium
160 under 12h:12h light-dark conditions, relative humidity of 70% and at 25° C. The
161 Clomeleon DNA construct (Kuner and Augustine, 2000), kindly provided by Thomas
162 Kuner, was inserted into the pUAST vector (Brand and Perrimon, 1993) via the
163 EcoRI and XhoI restriction sites. Transgenic constructs were injected by Genetic

164 Services Inc. (Cambridge, MA) into *yw* embryos using standard procedures and
165 single transformants were outcrossed to autosomal balancers for chromosomal
166 mapping. Two independent insertions on different chromosomes were combined.
167 Homozygous female flies, 6-10 days old, carrying four copies of the UAS:Clomeleon
168 transgenes, were used for all imaging experiments. The fly strain *UAS-Cameleon 2.1*
169 (Fiala et al., 2002) was chosen for monitoring odor-evoked Ca^{2+} signals as an
170 appropriate FRET-based sensor comparable in its chromophores with Clomeleon.
171 *Orco-Gal4* (RRID:BDSC_23292, (Wang et al., 2003)), *Or22a-Gal4*
172 (RRID:BDSC_9951, (Vosshall et al., 2000)) and *GH146-Gal4* (RRID:BDSC_30026,
173 (Stocker et al., 1997)) were used to drive expression of *UAS-Clomeleon* or *UAS-*
174 *Cameleon* (RRID:BDSC_6901).
175
176 **Optical imaging**
177 For imaging intracellular Cl^- and Ca^{2+} dynamics in the AL, flies were restrained in
178 custom-built holders and a small window was cut into the head capsule. The hole
179 was covered with physiological saline solution, and imaging was performed using a
180 water immersion objective directly positioned above the exposed brain. Pharmaca
181 (GABA, potassium gluconate, PTX, NPPB) were applied by exchanging the saline
182 drop on the brain by a drop of the approximate volume and the targeted
183 concentration. For NPPB an additional ethanol application was carried out to control
184 for the solvent effect (data not shown). For transcuticular antennal imaging
185 (Kamikouchi et al., 2010), flies were restrained as for the *in vivo* dissection method
186 without opening the head capsule. Or22a-expressing OSNs were imaged from the
187 posterior side, while the majority of OSNs using *Orco-Gal4* were recorded from the
188 anterior side.

189 Imaging experiments were performed using TillPhotonics imaging equipment
190 (TILL imago, Till Photonics GmbH) with a CCD-camera (PCO imaging, Sensicam)
191 and a fluorescence microscope (Olympus, BX51WI) equipped with a 20x water
192 immersion objective (NA 0.95, XLUM Plan FI, Olympus) for AL imaging and a 10x air
193 objective (NA 0.30, UPlan FLN, Olympus) for antennal imaging. A monochromator
194 (Polychrome V, Till Photonics) provided light at 440 nm excitation wavelength which
195 was guided through a 470 nm dichroic short pass filter. The beam-splitter (Optical
196 Insights, DV-CC) separated YFP from CFP emission with a 505 DCXR and narrowed
197 the emissions with bandpass filters of 535/30 nm for YFP and 465/30 nm for CFP.
198 Images of both emitted wavelengths were projected side by side onto a single CCD
199 camera chip (PCO Imaging, Sensicam). Fourfold binning on the CCD-camera chip
200 resulted in an image size of 344 x 260 pixels with 1 pixel corresponding to 1.25 x
201 1.25 µm. Each recording lasted for 20 s with an acquisition rate of 2 Hz. Since
202 Clomeleon yielded a very low signal-to-noise ratio, we had to apply long exposure
203 times which limited our recording frequency. We also performed experiments with
204 the usually used frequency of 4Hz, resulting in weaker signal intensities and a lower
205 dynamic range. Since these signals did not reveal different temporal patterns in the
206 odor-evoked responses as the slower recorded signals, we decided in favor of an
207 increased signal-to-noise ratio and maintained a recording frequency of 2Hz for the
208 whole study. Odors were applied 2 s after experiment onset and lasted for 2 s.
209 Individual flies were imaged for up to 1 h, with interstimulus time intervals of 1-3 min.
210

211 **Odor stimulation**

212 Pure odorants were diluted in mineral oil (BioChemika Ultra; odor CAS: ethyl-3-
213 hydroxybuytrate: 5405-41-4, benzaldehyde: 100-52-7, acetic acid: 64-19-7, cis-

214 vaccenylacetate: 6186-98-7, pentyl acetate: 628-63-7, 1-hexanol: 111-27-3, ethyl
215 benzoate: 93-89-0). For use, 6 µl of 1:10 diluted odor was pipetted onto a small
216 piece of filter paper (100 mm^2, Whatman), which was inserted into a glass Pasteur
217 pipette. A stimulus controller (Syntech, Stimulus Controller CS-55) was used to apply
218 the odor in a continuous airstream at 1 l/min, monitored by a flow meter (Cole
219 Parmer). An acrylic glass tube guided the airflow to the fly antennae. Two additional
220 air sources (airflow 0.5 l/min) were connected to the tube and the stimulus controller.
221 One of them consisted of the glass pipette containing the odor on filter paper and
222 was hooked up for odor application, whereas the other pipette was empty and added
223 clean air to the continuous airstream forming an air equation which was switched off
224 during odor application.
225
226 **Data analysis**
227 Data were analyzed using custom-written IDL software (ITT Visual Information
228 Solutions). First, a rigid registration was accomplished for all recordings separately to
229 minimize movement artifacts throughout the time series. Second, the ratio of the two
230 fluorescent signals was calculated as F_{YFP}/F_{CFP} for every time point. The ratio (R)
231 represents the relative magnitude of the signal intensity. To achieve a comparable
232 standard for the calculation of the relative fluorescence changes of the ratio ($\Delta R/R$),
233 the fluorescence background was subtracted from the averaged values of frames 0
234 to 5 in each measurement, such that baseline fluorescence was normalized to zero.
235 The false color-coded fluorescence changes in the raw-data images were calculated
236 as the delta of frame 5 and 30 (Clomeleon) and frame 5 and 15 (Cameleon). Specific
237 time traces of a measurement depict the mean of a 7 x 7 pixel coordinate (i.e. 9 x 9
238 µm), which was positioned into an anatomically identified glomerulus and plotted as

239 a function over time. Since *GH146-Gal4* does not label glomeruli VM5d and VM5v,
240 these could not be characterized at the PN level (Grabe et al., 2015). To generate
241 schematic AL maps, the mean value of frames 10-30 for Clomeleon and 10-15 for
242 Cameleon of a specific glomerulus and odor was averaged over all animals imaged.
243 Although the chloride and calcium kinetics are clearly odor induced, they develop
244 very slowly over time and show their maximal response change after odor offset. We
245 therefore selected a delayed time window for our signal evaluation to capture the
246 maximum/minimum of the odor-induced responses. One has to keep in mind that the
247 monitored Ca^{2+} and Cl^{-} dynamics are also dependent on the kinetics and
248 concentrations (i.e. expression levels) of the fluorescent sensors and might not
249 reflect accurately the physiological time traces. However, this issue is more relevant
250 for fast stimulus dynamics (Martelli and Fiala, 2019), while with regard to slow
251 recording frequencies, as used here, the resulting kinetics of Cl^{-} and Ca^{2+} binding
252 are rather negligible.

253 Responses in each fly were normalized to the highest Cl^{-} or Ca^{2+} signal in
254 each animal over all odors. To extract the temporal aspect of odor separation in the
255 different neuronal populations, Euclidean distances (*L*2-Norm) were calculated. To
256 compare the results, we always used the same set of 11 identified glomeruli in each
257 data set. For a given stimulus *a*, the n-dimensional population vector (v^a) was
258 constructed using the relative fluorescence changes over time. Then the population
259 vectors of two stimuli, *a* and *b*, were used to calculated the distance for every single
260 data point (time) in the 40 frames as follows: $d(t) = (\Sigma(v_i^a(t) - v_i^b(t))^2)^{1/2}$, where *i* is an
261 index for the i-th glomerulus. In addition to the Euclidean distances, principal
262 component analysis was used to visualize the population activity of OSNs and PNs
263 depending on the imaged reporter protein. Taken together, the first three principal

264 components (**Figure 7C**) account for 67.3% (OSNs: Cameleon), 67.4% (OSNs:
265 Clomeleon), 79.7% (PNs: Cameleon) and 59% (PNs: Clomeleon) of the variation in
266 the related data set. Population vectors of all odor stimulations were aligned, taking
267 into account time as the source of sample points, and number of glomeruli as the
268 dimension of the original component space using the MatLab statistical toolbox. All
269 statistical analyses were performed using GraphPad InStat 3 as specified in each
270 figure legend.
271

272 **Results**

273 **Clomeleon as an indicator of intracellular Cl^- dynamics in olfactory neurons**

274 We generated flies carrying the genetically encoded Cl^- sensor Clomeleon (Kuner
275 and Augustine, 2000) in order to visualize *in vivo* Cl^- mediated inhibitory responses in
276 the olfactory system. Using the binary GAL4-UAS transcriptional system (Brand and
277 Perrimon, 1993), we expressed Clomeleon in the majority of OSNs using *Orco-Gal4*
278 (Wang et al., 2003) and in PNs using *GH146-Gal4* (Stocker et al., 1997) (**Figure**
279 **1A,B**). To test whether Clomeleon is functional in *Drosophila* olfactory neurons, we
280 optically monitored fluorescence changes in OSNs and PNs in the AL, while we
281 applied potassium gluconate (KGlu) to induce neuronal excitation globally and,
282 concomitantly, inhibition through LN input onto OSNs and PNs (**Figure 1C-F**; see
283 network scheme in **Figure 2A**). Applying KGlu increased CFP fluorescence, while
284 YFP fluorescence was strongly decreased; thereby, the YFP/CFP ratio was reduced.
285 To verify that this reflected inhibition, we applied the inhibitory transmitter γ-
286 aminobutyric acid (GABA). GABA application immediately reduced the YFP/CFP
287 ratio in both OSNs and PNs (**Figure 1G,H**). Notably, we observed a second, strong
288 emission decrease which was delayed by about 35 s. The source of this second

289 decrease is yet unclear, but could be due to the slow diffusion rate of GABA as it is
290 bath applied to the whole brain and not actively perfused. The gradually increasing
291 GABA concentration might surpass a threshold that initiates a strong inhibition
292 reflected by the second phase. In combination with a gradual desensitization towards
293 GABA (Hong and Wilson, 2015), this could explain the observed slow and biphasic
294 GABA effect. To confirm that these ratio changes were dependent on Cl^-, we
295 removed Cl^- from the saline solution covering the fly's brain. Odor application before
296 Cl^- removal induced a clear ratio change, which was significantly reduced using Cl^--
297 free saline (**Figure 1I**). To further verify that our reporter was reflecting the
298 intracellular Cl^- concentration, we applied the chloride channel blocker 5-nitro-2(-3-
299 phenylpropylamine) benzoic acid (NPPB) to block Cl^- channels in *Drosophila*
300 neurons (O'Donnell et al., 1998). As expected, application of NPPB strongly reduced
301 the Cl^- influx which was partly reversibly (**Figure 1J**).

302 Since the YFP fluorescence has been reported to be affected by the pH value
303 at $[Cl^-]_i$ above 50 mM (Kuner and Augustine, 2000), we confirmed that the
304 fluorescence emission was not influenced by pH changes within the physiologically
305 relevant range of 6.9 to 7.3 (**Figure 1K**). This is in accordance with the described $[Cl^-$
306 $]_i$ in OSNs, which is ~24 mM in moths (Steinbrecht, 1992) and ~20 mM in flies
307 (Reinert et al., 2011). Therefore, a potential influence of pH changes on Clomeleon
308 is negligible. Overall, our results confirm that Clomeleon functions reliably as a Cl^-
309 indicator in olfactory neurons of the *Drosophila* AL.

310

311 **Odor stimulation induces peripheral Cl^- influx in dendrites of OSNs**

312 Next, we analyzed whether odor stimulation causes a Cl^- increase at the most
313 peripheral level of sensory transduction and performed transcuticular Cl^- imaging in

314 OSN dendrites located on the fly's antenna (**Figure 2A,B**). Odor stimulation induced
315 an odor-specific, spatially confined increase in $[Cl^-]_i$. These spatially restricted signals
316 correspond to distinct sensillum types, which have well-described, specific
317 distributions on the third antennal segment (Shanbhag et al., 1999; Grabe et al.,
318 2016) (**Figure 2C,D**). In order to determine which sensillum types were excited by
319 the odors used, we performed Ca^{2+} imaging in comparison using the ratiometric Ca^{2+}
320 indicator Cameleon 2.1 (Miyawaki et al., 1999). Cl^- signals are characterized by a
321 reduction in the Clomeleon's YFP/CFP ratio (= increase in $[Cl^-]_i$) whereas Ca^{2+}
322 signals were indicated by a ratio increase in the Cameleon's YFP/CFP ratio (=
323 increase in $[Ca^{2+}]_i$) (**Figure 2D**). Notably, some odors, such as ethyl-3-
324 hydroxybutyrate, evoked both a Ca^{2+} and a Cl^- signal in the same areas of the
325 antennal surface, indicating a concomitant Ca^{2+} and Cl^- influx in OSNs. Other
326 odorants, e.g., benzaldehyde, induced spatially non-overlapping Cl^- and Ca^{2+} signals,
327 indicating independent excitation and inhibition events in distinct sensilla (**Figure 2D**).
328 This separation of inhibition and excitation is underlined by the strong Cl^- increase
329 induced by acetic acid in the tip region of the antenna without significant Ca^{2+}
330 responses (**Figure 2E**). Acetic acid activates solely OSNs present in one type of
331 coeloconic sensilla (Abuin et al., 2011), which is not labeled by the *Orco-Gal4* line.
332 To verify that the observed antennal Cl^- signals indeed reflect neuronal inhibition, we
333 expressed Clomeleon selectively in OSNs expressing Or47b. OSNs expressing this
334 receptor selectively respond to the pheromone methyl laurate and are mainly
335 inhibited by other odors (Hallem and Carlson, 2006; Dweck et al., 2015). Application
336 of the odor ethyl-3-hydroxybutyrate, which induces an inhibition of Or47b-expressing
337 OSNs as shown via single-sensillum recordings (Hallem and Carlson, 2006), leads
338 to a strong and long-lasting Cl^- influx in this OSN type (**Figure 2F**).

339 We next wondered whether the odor-induced antennal Cl^- increase derives
340 within the sensillum and can be attributed to OSN dendrites or whether these signals
341 rather reflect a feedback inhibition from the AL. We therefore monitored Cl^- signals
342 following odor stimulation while we abolished any feedback signaling from the AL by
343 cutting the antennal nerve (**Figure 2G**). Interestingly, this treatment significantly
344 reduced Cl^- signals in the antenna, but did not abolish them. This result
345 demonstrates Cl^- conductivity in dendrites of OSNs, indicating that Cl^- channels are
346 present in OSNs and localized to the most peripheral dendritic compartments in the
347 fly antenna. However, at the same time we do not exclude an additional feedback
348 inhibition from the AL.
349

350 **Cl^--dependent, inhibitory odor maps in OSN terminals in the AL**

351 Within the AL, OSNs are presynaptically inhibited by GABAergic LNs (Olsen and
352 Wilson, 2008; Root et al., 2008; Mohamed et al., 2019) with varying and glomerulus-
353 specific GABA sensitivities (Hong and Wilson, 2015). In order to visualize odor-
354 evoked inhibition at the level of the axonal termini across multiple glomeruli, we
355 performed Cl^- imaging in presynaptic OSN axons in the AL using an *in vivo*
356 preparation (Strutz et al., 2012) (**Figure 3A**). Due to the stereotypy of the glomerular
357 AL morphology, we could reliably identify individual glomeruli in each animal using
358 digital AL atlases (Laissue et al., 1999; Couto et al., 2005) (**Figure 3B**). Each odor
359 stimulation induced a specific combinatorial pattern of inhibited glomeruli, which was
360 stereotypic among individuals (**Figure 3C, Figure 6**). The time courses of YFP/CFP
361 ratio changes in selected glomeruli revealed odor-specific and glomerulus-specific
362 Cl^- influx (**Figure 3D**). However, a time-resolved analysis across multiple glomeruli
363 showed that Cl^- signals are detected in all glomeruli optically accessible during the

364 imaging experiments (**Figure 3E**). In conclusion, strong and odor-specific inhibition
365 of distinct glomeruli is accompanied by less intense, global inhibition across the
366 entire OSN population. The Cl^- signals that were optically monitored lasted until the
367 end of each measurement, i.e., they strongly outlasted the 2 s odor stimulation.
368 Therefore, we examined how much time was required before the Clomeleon signal
369 returned to baseline (**Figure 3F-H**). Odor application with different inter-stimulus
370 intervals revealed that even though the fluorescence emission ($\Delta R/R$) continued to
371 drop after stimulation, repetitive odor stimulation still elicited further Clomeleon
372 signals after 10 or 60 s (**Figure 3F,G**). A complete recovery of the Clomeleon
373 fluorescence was not observed before 120 s after odor stimulation had elapsed
374 (**Figure 3H**). The actual kinetics of any fluorescence sensor depend on multiple
375 factors, e.g., the concentration of the sensor determined by the expression level, the
376 affinity of the sensor to its ligand, or the dynamic range of the sensor. Therefore, it is
377 difficult to conclude to what degree the dynamics of Cl^- transients quantitatively
378 reflect the actual balance between Cl^- influx and intracellular Cl^- removal. However, a
379 slow recovery of Clomeleon signals has also been observed in mammalian neurons
380 (Kuner and Augustine, 2000; Berglund et al., 2006) and has been attributed to the
381 slow removal of $[Cl^-]_i$ by transporters rather than kinetic properties of the Cl^- sensor
382 (Staley and Proctor, 1999; Berglund et al., 2009; Berglund et al., 2016). It is
383 therefore quite conceivable that the odor-evoked Cl- transients in OSNs indeed
384 strongly outlast the actual stimulation.
385

386 **Comparison between odor-evoked Cl^- signaling in OSN dendrites and axons**

387 As shown so far, odors induce a clear Cl^- increase at the level of the peripheral
388 signal input, i.e., in the antenna (**Figure 2**), and at the sites of synaptic transmission,

389 i.e., in OSNs of the AL (**Figure 3**). To examine the relationship between these two
390 signal sources in more detail, we comparatively monitored odor-evoked $[Cl^-]_i$ and
391 $[Ca^{2+}]_i$ of a single OSN population at its dendrites and axonal termini. This was
392 achieved by selective expression of Clomeleon or Cameleon, respectively, in OSNs
393 expressing the odorant receptor Or22a, which targets the glomerulus DM2 (Couto et
394 al., 2005; Fishilevich and Vosshall, 2005). As described previously (Pelz et al., 2006),
395 a strong excitatory Ca^{2+} response was elicited by methyl hexanoate, while ethyl-3-
396 hydroxybutyrate induced an intermediate, and benzaldehyde no significant response
397 (**Figure 4A,B**). The relative intensities of odor-evoked Ca^{2+} responses did not differ
398 between antenna and AL (**Figure 4C**). However, all three odors induced
399 comparatively strong Cl^- responses in the fly antenna (**Figure 4A, *lower panel***),
400 while only methyl hexanoate, one of the most potent activators of this OSN type,
401 elicited a significant Cl^- response at the AL level (**Figure 4B, *lower panel*, Figure**
402 **4D**). Hence, the intensity of odor-evoked Cl^- influx at the level of OSN dendrites and
403 somata is relatively independent of the actual intensity of the accompanying Ca^{2+}
404 influx. On the contrary Cl^- mediated inhibition in the AL reflects more odor-specific
405 inhibition.
406
407 **Cl^--dependent, inhibitory odor maps in projection neuron terminals in the AL**
408 In order to analyze inhibitory patterns of output neruons in the AL, we performed Cl^-
409 imaging at the dendrites of PNs using the enhancer trap line *GH146-Gal4* that labels
410 the majority of uniglomerular PNs (Stocker et al., 1997). Odor application induced
411 clear spatially confined and odorant-specific patterns of inhibition that could be
412 assigned to identified glomeruli (**Figure 5A,B**). A time-resolved analysis across all
413 glomeruli revealed a strongly pronounced Cl^- influx in a glomerulus- and odor-

414 specific manner, and typically with some delay after odor onset (**Figure 5C).** These
415 odor-specific, inhibitory patterns evolve slowly over time and persist until the end of
416 the measurement, as it is the case at the OSN level. Notably, we observed a
417 concordance in the Cl^- responses between OSNs and PNs, in a way that a given
418 odor inhibited the same glomeruli at the input and the output level of the AL (**Figure**
419 **3E**, and **Figure 5C**). However, this correlation was only apparent for strongly
420 inhibited glomeruli, while weaker Cl^- responses occurred in more glomeruli at the PN
421 level when compared to OSNs. Again, this indicates a dual role of Cl^--mediated
422 inhibition, i.e., a moderate, global inhibition and a strong odor- and glomerulus-
423 specific inhibition, potentially reflecting the various types of inhibitory neurons in the
424 AL, the global and patchy GABAergic LNs (Chou et al., 2010; Mohamed et al., 2019).
425 Since the spatio-temporal activity of PN ensembles is influenced by inhibitory,
426 GABAergic LNs (Wilson and Laurent, 2005), we tested whether the Clomeleon
427 signals were dependent on GABA receptors. Therefore, we performed Cl^- imaging
428 experiments after silencing the inhibitory LN input by applying the $GABA_A$-type
429 antagonist picrotoxin (5μM) that blocks ionotropic Cl^--ion channels. In addition to
430 $GABA_A$ receptors, picrotoxin has been shown to block also glutamate-gated chloride
431 channels (GluCl) (Liu and Wilson, 2013). However, at the low concentration used in
432 this study the antagonist mainly functions as a $GABA_A$ antagonist without affecting
433 GluCl channels (Hong and Wilson, 2015). Application of picrotoxin led to a significant
434 reduction of the odor-induced Cl^- signals by on average 59% (**Figure 5D**). This result
435 indicates that the $GABA_A$ receptor contributes to the Cl^- mediated inhibition at the AL
436 output level.
437

438 **A comparative functional map of odor-evoked activation and inhibition in the**
439 **antennal lobe**

440 We next examined the overlap of the odor-evoked inhibitory patterns compared to
441 the spatial patterns of glomerular Ca^{2+} activities. Therefore, we performed functional
442 imaging experiments to a variety of different odors and monitored odor-evoked Ca^{2+}
443 as well as Cl^- responses by expressing Cameleon or Clomeleon in OSNs and PNs,
444 respectively. Subsequently, we mapped the odor-induced responses to identified
445 glomeruli to generate a functional AL atlas (**Figure 6**). First, we observed that, in the
446 majority of cases, the odor-evoked maps of excitation and inhibition closely match at
447 the input and the output level, i.e., those glomeruli which were excited were also
448 often inhibited by a certain odor. Such a concordance suggests a gain control
449 mechanism for odor-induced excitation as described for the OSN level (Olsen and
450 Wilson, 2008), which should occur in all glomeruli receiving an excitatory input.
451 Second, we observed that some glomeruli were inhibited without being excited. This
452 finding suggests a second role of Cl^- mediated inhibition in the *Drosophila* AL which
453 could contribute to confining the spatio-temporal patterns, resulting in an enhanced
454 contrast between different odor representations as shown for the honeybee AL
455 (Sachse and Galizia, 2002). Notably, we never observed glomeruli, which were
456 excited without being inhibited.

457

458 **Input-output transformation**

459 Last, we analyzed the difference between the odor-evoked representations of input
460 and output neurons for a subgroup of 11 glomeruli that could be unambiguously
461 identified in each experiment (**Figure 7A**). Since each fluorescent reporter protein
462 exhibits different kinetics, one has to be careful when comparing temporal dynamics

463 between different sensors. We therefore compared temporal aspects of odor-evoked
464 responses of different processing levels for one reporter protein only. Quantification
465 of the evoked mean responses to specific odors showed that excitatory as well as
466 inhibitory odor responses were, on average, stronger at the PN level than at the
467 OSN level (**Figure 7B**) which is well in line with electrophysiological recordings
468 (Wilson and Laurent, 2005; Bhandawat et al., 2007; Seki et al., 2017). To visualize
469 how the odor-specific responses evolve over time, we applied principal component
470 analyses to reduce the multidimensional, spatio-temporal activity/inhibition to three
471 dimensions and illustrated the odor-evoked ensemble activity as trajectories over
472 time (**Figure 7C**). Independent of the reporter protein, different odors evoked distinct
473 trajectories, which demonstrates an odor-specific separation of Ca^{2+} as well as Cl^{-}
474 responses at both processing levels, i.e., OSNs and PNs. To quantify how fast this
475 odor separation evolved, we calculated Euclidean distances between the population
476 vectors of the different odor representations for Cameleon and Clomeleon signals,
477 respectively (**Figure 7D,E**, upper panels). Interestingly, PN responses revealed in
478 general lower Euclidean distances than OSN responses. Although PNs showed an
479 increased level of inhibition, PNs exhibited generally broader odor-evoked responses
480 compared to OSNs (Wilson et al., 2004; Seki et al., 2017). This broadening leads to
481 broader odor tuning curves and a stronger overlap of odor representations at the PN
482 level (Niewalda et al., 2011; Schubert et al., 2014; Seki et al., 2017), while PN
483 responses show a higher degree of odor categorization according to behaviorally
484 meaningful values (Niewalda et al., 2011; Knaden et al., 2012).

485 After normalizing all pair-wise Euclidean distances, we calculated the
486 latencies to the half maximum odor separation (**Figure 7D,E**, lower panel) and
487 observed that it was reached significantly earlier in PNs than in OSNs. This finding is

488 in accordance with electrophysiological recordings in *Drosophila* showing that PN
489 responses have shorter latencies to reach 90% of their response peak than OSNs
490 (Bhandawat et al., 2007) indicating that PNs act as high-pass filters that rapidly
491 convey rising OSN responses to third-order neurons. When considering the chloride
492 responses, this latency shift is even more pronounced for Cl^- signals. This
493 observation is most likely due to reciprocal inhibitory mechanisms that differently
494 affect OSN and PN responses: PNs are inhibited by fast forward inhibition from
495 OSNs via GABAergic LNs (Wilson and Laurent, 2005) before OSNs receive
496 presynaptic feedback inhibition from PNs through, in turn, GABAergic LNs (Olsen
497 and Wilson, 2008; Root et al., 2008).
498

499 **Discussion**

500 **Clomeleon-based Cl^- imaging in the *Drosophila* nervous system**

501 Hardly any optical imaging technique reaches the unmatched temporal precision of
502 electrophysiological recordings as yet, and the determination of membrane potential
503 changes represents the most accurate approach to determine how sensory stimuli
504 are represented by single or small groups of neurons (Wilson et al., 2004; Wilson
505 and Laurent, 2005; Seki et al., 2017). Optical imaging, on the contrary, offers the
506 advantage of monitoring physiological parameters that correlate with membrane
507 potential changes across spatio-temporally distributed populations of neurons
508 (Ahrens et al., 2013; Chen et al., 2013). Membrane depolarization is typically
509 accompanied by increases in intracellular Ca^{2+} from a variety of sources, and Ca^{2+}
510 imaging represents currently the "gold standard" for visualizing neuronal excitation in
511 *Drosophila* (Riemensperger et al., 2012). However, neuronal inhibition, most often
512 mediated by Cl^- influx, is not directly captured using Ca^{2+} imaging. Establishing

513 Clomeleon as a tool for monitoring Cl^- dynamics both in the peripheral and central
514 nervous system provides an important step towards filling this gap. Its ratiometric
515 nature as a FRET-based sensor demands some additional considerations in contrast
516 to single chromophore sensors such as calcium reporters belonging to the GCaMP
517 family (Tian et al., 2009). Especially the size, pH sensitivity, and slow response
518 dynamics require the future development of a single chromophore chloride sensor,
519 which hopefully eases its applicability. The development of the Cl^- sensor
520 SuperClomeleon, which still represents a FRET-based sensor, reveals an improved
521 signal-to-noise ratio and needs to be established for the *Drosophila* olfactory system
522 (Grimley et al., 2013).

523 It is important to consider that the monitored changes in intracellular Ca^{2+} and
524 Cl^- derive from different cell processes within the neurons. Recorded changes in
525 Ca^{2+} and Cl^- can therefore depend on fluxes at the synapse or along the neuron, as
526 well as release from intracellular calcium stores, which are mediated by ligand-gated
527 as well as voltage-gated Ca^{2+} and Cl^- channels in insects (Messina et al., 1996;
528 Wicher et al., 2001; Fiala and Spall, 2003; Flores et al., 2006; Pézier et al., 2010).
529 Since the temporal resolution in functional imaging recordings is rather low
530 compared to electrophysiological recordings, the different dynamics of these ion
531 channels are not visible in the fluorescence signal of the different sensors.

532

533 **Is Cl^- influx part of the olfactory signal transduction in insects?**

534 We observed an odor-evoked Cl^- influx in OSN dendrites of the *Drosophila* antenna.
535 In vertebrates, Cl^--conductance is an integral component of the canonical olfactory
536 signal transduction cascade (Labarrera et al., 2013). Here, odor stimulation leads to
537 a membrane-current composed of a cationic and a delayed Cl^- component

538 (Kurahashi and Yau, 1993). Although Cl^--conductance is in most cases associated
539 with neuronal inhibition, this Cl^- current amplifies the olfactory signal by Cl^- efflux
540 through a Ca^{2+}-activated Cl^- channel which is most likely mediated by anoctamin-2
541 (ANO2) (Lowe and Gold, 1993; Stephan et al., 2009; Delgado et al., 2016). The
542 insect olfactory signal transduction is crucially different from that of vertebrates in two
543 aspects: First, olfactory receptors of the OR and IR type are ionotropic receptors
544 mediating excitatory cation influx (Sato et al., 2008; Wicher et al., 2008; Rytz et al.,
545 2013). Metabotropic signaling cascades have been clearly described for insect
546 OSNs, but their exact modulatory functions remain unclear as yet (Wicher et al.,
547 2008). Second, the equilibrium potential of Cl^- (E_{Cl}) in insect OSNs differs from that
548 of vertebrates. Since $[Cl^-]_i$ is lower than in the extracellular medium, as shown in
549 moths (Steinbrecht, 1992), the electromotive force will lead to a Cl^- influx, if the
550 membrane potential is shifted above E_{Cl} (i.e. -36 mV). Hence, when OSNs become
551 excited, a Cl^- influx through Ca^{2+}-activated Cl^- channels might result in
552 hyperpolarization of the plasma membrane (Pézier et al., 2010).

553 Interestingly, dendrites of moth OSNs express an analogous Ca^{2+}-activated
554 Cl^- channel that functionally resembles ANO2 (Pézier et al., 2010). The *Drosophila*
555 *melanogaster* genome contains two different ANO2 orthologues (CG6938, CG10353)
556 whose molecular function has, however, not yet been studied. Further experiments
557 are needed to analyze the role of ANO2 in odor-evoked Cl^- dynamics in *Drosophila*
558 OSNs. The fact that the antennal Cl^- influx co-occurred frequently with a Ca^{2+} influx
559 further suggest the existence of Ca^{2+}-activated Cl^- channels in the antenna. This type
560 of Cl^--mediated inhibition might reflect shunting inhibition as a mechanism for gain
561 control leading to stabilization of odor-evoked excitation (Wilson and Mainen, 2006).

562 In addition, we also observed Cl^- influx that was not directly correlated with the
563 excitation of the respective OSNs, reflecting a second type of Cl^- mediated inhibition.
564 This finding suggests either again the existence of Cl^--channels in OSN dendrites or,
565 alternatively, a retrograde diffusion of Cl^- from the AL. Interestingly, when we
566 abolished any feedback signaling from the AL we still observed Cl^- influx, supporting
567 the first assumption. However, since the Cl^- signals were not identical but reduced,
568 we assume that Cl^- dynamics in OSN dendrites are partly influenced by Cl^- influx into
569 OSN axonal termini in the AL. The latter assumption is further supported by our
570 observation that applying GABA to the AL induced a significant Cl^- influx in the
571 antenna (data not shown).

572 The comprehensive study by Hallem and Carlson on receptor-ligand
573 interactions where a widespread inhibition below baseline firing rates among one
574 third out of 24 selectively expressed ORs was observed (Hallem and Carlson, 2006),
575 is well in line with our observation of inhibitory odor responses in the *Drosophila*
576 antenna. Interestingly, OSNs expressing Or47b - known to selectively respond to the
577 pheromone methyl laurate (Dweck et al., 2015) - were never excited by the large
578 odor set tested in the aforementioned study, but showed inhibitory responses to 34%
579 of the odors. Those OSNs target glomerulus VA1d, and we indeed observed clear
580 odor-evoked Cl^- responses in VA1d, while Ca^{2+}-influx did never occur. In addition, Cl^-
581 imaging of Or47b-expressing OSNs on the antenna confirms the odor-induced
582 inhibition of this OSN type. As a second example, benzaldehyde elicited a strong Cl^-
583 influx in OSNs expressing Or22a in the antenna without being accompanied by a
584 Ca^{2+} influx. This odor has already been characterized as an Or22a-inhibitor (Pelz et
585 al., 2006; Wicher et al., 2008), which strongly suggests that our second type of Cl^-
586 mediated inhibition reflects hyperpolarization and thus odor-specific inhibition in the

587 antenna. Therefore, our study demonstrates that inhibitory odor responses of OSNs
588 are not only generated by a reduction in the intracellular cation concentration leading
589 to a reduced firing rate as widely assumed, but that they are also carried by an influx
590 of Cl^-. It still remains to be investigated how Cl^- channels are integrated in the
591 olfactory signal transduction machinery of insects.
592
593 **Multiple roles of Cl^- signaling at the antennal lobe network level**
594 Within the insect AL, odor representations are shaped by the inhibitory network of
595 various types of GABAergic LNs (Sachse and Galizia, 2002; Wilson and Laurent,
596 2005; Silbering and Galizia, 2007; Hong and Wilson, 2015; Mohamed et al., 2019). It
597 has been shown that OSNs are presynaptically inhibited by LNs, mediated by both
598 $GABA_A$ and $GABA_B$ receptors (Olsen and Wilson, 2008; Root et al., 2008). Since
599 $GABA_A$ receptors are ligand-activated Cl^- channels, they provide a direct molecular
600 substrate for the Cl^- influx in OSNs at the AL level. Likewise, PNs express both
601 $GABA_A$ and $GABA_B$ receptors (Enell et al., 2007), and their odor responses are
602 influenced by both receptor types (Wilson and Laurent, 2005; Silbering and Galizia,
603 2007). Here we confirm the contribution of $GABA_A$ receptors pharmacologically for
604 Cl^- influx. In addition, our data provide evidence that the synaptic inhibition of PNs is
605 stronger than that of OSNs, since we clearly see an increase in the number of
606 inhibited glomeruli from the input to the output level. However, one has to keep in
607 mind that the sensor dynamics might not reflect the potentially varying dynamics of
608 the membrane potential in these different neuron types. Chloride ions themselves
609 have their own dynamics, and potentially those dynamics reflect actual neuronal
610 dynamics only loosely. Still, our data demonstrates a transformation of odor
611 representations that is not accessible if only excitation-associated Ca^{2+} is taken into

account. Our findings suggest two distinct types of Cl^- signals in the AL, i.e., a global, moderate inhibition and a strong, cell-type-specific inhibition. This reflects the structural diversity of GABAergic LNs in the *Drosophila* AL (Chou et al., 2010; Seki et al., 2010; Hong and Wilson, 2015). The majority of LNs arborizes in most glomeruli, and therefore evenly distributes the input from most OSN types. Thus, we would expect that the level of inhibition in each glomerulus should mirror the level of activity in all glomeruli with varying sensitivities to the GABAergic input (Hong et al. 2015). This assumption provides a mechanism for global, inhibitory gain control at the cellular and network level to keep the olfactory circuitry in the operating state across odorant combinations and concentrations as shown for the zebrafish olfactory bulb (Zhu et al., 2013).

As a second type of Cl^- mediated inhibition, we observed Cl^- responses that were not linked to any excitation, and most likely reflect local inhibition that specifically shapes neuronal information processing, analogous to the mammalian system (Mori et al., 1999; Urban, 2002). In fact, heterogeneous populations of LNs innervating only few glomeruli also exist (Chou et al., 2010; Seki et al., 2010), which might provide the neuronal substrate for such glomerulus- and odor-specific inhibition. Along that line, recent data provide evidence that patchy, but not global GABAergic LNs accomplish selective lateral inhibition between specific glomeruli processing odors with opposing hedonic valences (Mohamed et al., 2019).

Temporal aspects of odor-evoked chloride responses

The measured odor-induced Cl^- and Ca^{2+} responses reveal different temporal dynamics. However, the temporal differences between Ca^{2+}- and Cl^--evoked signals are difficult to interpret because it is not clear whether they derive from different

637 reporter dynamics or indeed reflect physiological properties. Hence when
638 considering temporal dynamics, we restricted any comparison of data obtained to
639 only one reporter protein and therefore compared dynamics of input and output
640 neurons for Cameleon and Clomeleon separately.

641 Although the chloride influx is clearly odor-induced, it evolves slowly over time
642 and outlasts the odor stimulation period. Such long-lasting chloride responses are
643 consistent with observations in mammalian neurons (Kuner and Augustine, 2000;
644 Berglund et al., 2006) and might reflect the relatively slow rate of Cl^- removal from
645 the neurons (Staley and Proctor, 1999; Berglund et al., 2009; Berglund et al., 2016).
646 This slow recovery in the Cl^- response might affect the excitability of the neuron for a
647 period significantly outlasting the stimulation. However, as mentioned above, the
648 kinetics of fluorescence sensors depend on intrinsic parameters of the sensor itself
649 and firm conclusions about the exact kinetics about the Cl^- currents cannot be drawn
650 as yet.

651

652 **Determining Cl^- and Ca^{2+} representations together provide a more accurate**
653 **assessment of sensory processing**

654 The importance of synaptic inhibition for accurate behavioral responses to olfactory
655 stimuli has been demonstrated in different species. Mice show accelerated
656 discrimination ability when synaptic inhibition of mitral cells is increased by
657 selectively altering granule cell function (Abraham et al., 2010). In locusts and flies,
658 disruptive manipulation of the GABAergic AL network reduces the insects' ability to
659 behaviorally discriminate between similar odors (Stopfer et al., 1997; Barth et al.,
660 2014). The similarity between glomerular excitation patterns evoked by different
661 odors often matches with the animals' ability to discriminate between the odors in

662 behavioral tasks (Sachse and Galizia, 2003; Guerrieri et al., 2005; Niewalda et al.,
663 2011; Barth et al., 2014; Carcaud et al., 2018). In *Drosophila*, the spatiotemporal,
664 glomerular Ca^{2+} activity patterns at the PN level reflect more accurately the animals'
665 perception of similarities between odors than the patterns observed at the OSN level
666 (Niewalda et al., 2011). This difference between OSNs and PNs could, at least partly,
667 be due to the influence of GABA-mediated inhibition. Determining Cl^--mediated
668 inhibition across ensembles of neurons in addition to Ca^{2+}-mediated excitation
669 therefore enables us to more comprehensively and more accurately characterize
670 sensory processing underlying the perception of olfactory or other sensory stimuli.

671 **References**

672 Abraham NM, Egger V, Shimshek DR, Renden R, Fukunaga I, Sprengel R, Seeburg
673 PH, Klugmann M, Margrie TW, Schaefer AT, Kuner T (2010) Synaptic
674 Inhibition in the Olfactory Bulb Accelerates Odor Discrimination in Mice.
675 Neuron 65:399-411.
676 Abuin L, Bargeton B, Ulbrich MH, Isacoff EY, Kellenberger S, Benton R (2011)
677 Functional Architecture of Olfactory Ionotropic Glutamate Receptors. Neuron
678 69:44-60.
679 Ahrens MB, Orger MB, Robson DN, Li JM, Keller PJ (2013) Whole-brain functional
680 imaging at cellular resolution using light-sheet microscopy. Nature Methods
681 10:413.
682 Barth J, Dipt S, Pech U, Hermann M, Riemensperger T, Fiala A (2014) Differential
683 Associative Training Enhances Olfactory Acuity in *Drosophila melanogaster*. J
684 Neurosci 34:1819-1837.
685 Berglund K, Kuner T, Augustine GJ (2009) Clomeleon, a Genetically Encoded
686 Chloride Indicator. In: Physiology and Pathology of Chloride Transporters and
687 Channels in the Nervous System (Alvarez M, ed), pp 123-136.
688 Berglund K, Wen L, Dunbar RL, Feng G, Augustine GJ (2016) Optogenetic
689 Visualization of Presynaptic Tonic Inhibition of Cerebellar Parallel Fibers. J
690 Neurosci 36:5709-5723.
691 Berglund K, Schleich W, Krieger P, Loo L, Wang D, Cant N, Feng G, Augustine G,
692 Kuner T (2006) Imaging synaptic inhibition in transgenic mice expressing the
693 chloride indicator, Clomeleon. Brain Cell Biology 35:207-228.
694 Bhandawat V, Olsen SR, Gouwens NW, Schlief ML, Wilson RI (2007) Sensory
695 processing in the Drosophila antennal lobe increases reliability and
696 separability of ensemble odor representations. Nat Neurosci 10:1474-1482.
697 Brand AH, Perrimon N (1993) Targeted gene expression as a means of altering cell
698 fates and generating dominant phenotypes. Development 118:401-415.
699 Carcaud J, Giurfa M, Sandoz J-C (2018) Differential Processing by Two Olfactory
700 Subsystems in the Honeybee Brain. Neuroscience 374:33-48.
701 Chen T-W, Wardill TJ, Sun Y, Pulver SR, Renninger SL, Baohan A, Schreiter ER,
702 Kerr RA, Orger MB, Jayaraman V, Looger LL, Svoboda K, Kim DS (2013)
703 Ultrasensitive fluorescent proteins for imaging neuronal activity. Nature
704 499:295.
705 Chou Y-H, Spletter ML, Yaksi E, Leong JCS, Wilson RI, Luo L (2010) Diversity and
706 wiring variability of olfactory local interneurons in the Drosophila antennal lobe.
707 Nat Neurosci 13:439-449.
708 Couto A, Alenius M, Dickson BJ (2005) Molecular, anatomical, and functional
709 organization of the *Drosophila* olfactory system. Curr Biol 15:1535-1547.
710 Delgado R, Mura CV, Bacigalupo J (2016) Single Ca2+-activated Cl− channel
711 currents recorded from toad olfactory cilia. BMC Neuroscience 17:17.
712 Duebel J, Haverkamp S, Schleich W, Feng G, Augustine GJ, Kuner T, Euler T
713 (2006) Two-Photon Imaging Reveals Somatodendritic Chloride Gradient in
714 Retinal ON-Type Bipolar Cells Expressing the Biosensor Clomeleon. Neuron
715 49:81-94.
716 Dweck HKM, Ebrahim SAM, Thoma M, Mohamed AAM, Keesey IW, Trona F,
717 Lavista-Llanos S, Svatoš A, Sachse S, Knaden M, Hansson BS (2015)
718 Pheromones mediating copulation and attraction in Drosophila. Proc Natl
719 Acad Sci 112:E2829-E2835.

720 Egger V, Urban NN (2006) Dynamic connectivity in the mitral cell–granule cell
721 microcircuit. Semin Cell Dev Biol 17:424-432.
722 Enell L, Hamasaka Y, Kolodziejczyk A, Nässel DR (2007) γ-Aminobutyric acid
723 (GABA) signaling components in Drosophila: Immunocytochemical
724 localization of GABAB receptors in relation to the GABAA receptor subunit
725 RDL and a vesicular GABA transporter. J Comp Neurol 505:18-31.
726 Fiala A, Spall T (2003) In Vivo Calcium Imaging of Brain Activity in Drosophila by
727 Transgenic Cameleon Expression. Sci STKE 2003:pl6-.
728 Fiala A, Spall T, Diegelmann S, Eisermann B, Sachse S, Devaud JM, Buchner E,
729 Galizia CG (2002) Genetically expressed cameleon in *Drosophila*
730 *melanogaster* is used to visualize olfactory information in projection neurons.
731 Curr Biol 12:1877-1884.
732 Fishilevich E, Vosshall LB (2005) Genetic and functional subdivision of the
733 *Drosophila* antennal lobe. Curr Biol 15:1548-1553.
734 Flores CA, Niemeyer MI, Sepúlveda FV, Cid LP (2006) Two splice variants derived
735 from a Drosophila melanogaster candidate ClC gene generate ClC-2-type Cl−
736 channels. Molecular Membrane Biology 23:149-156.
737 Glykys J, Dzhala VI, Kuchibhotla KV, Feng G, Kuner T, Augustine G, Bacskai BJ,
738 Staley KJ (2009) Differences in Cortical versus Subcortical GABAergic
739 Signaling: A Candidate Mechanism of Electroclinical Uncoupling of Neonatal
740 Seizures. Neuron 63:657-672.
741 Grabe V, Strutz A, Baschwitz A, Hansson BS, Sachse S (2015) Digital in vivo 3D
742 atlas of the antennal lobe of Drosophila melanogaster. J Comp Neurol 523.
743 Grabe V, Baschwitz A, Dweck Hany KM, Lavista-Llanos S, Hansson Bill S, Sachse S
744 (2016) Elucidating the Neuronal Architecture of Olfactory Glomeruli in the
745 Drosophila Antennal Lobe. Cell Reports 16:3401-3413.
746 Grienberger C, Konnerth A (2012) Imaging Calcium in Neurons. Neuron 73:862-885.
747 Grimley JS, Li L, Wang W, Wen L, Beese LS, Hellinga HW, Augustine GJ (2013)
748 Visualization of Synaptic Inhibition with an Optogenetic Sensor Developed by
749 Cell-Free Protein Engineering Automation. J Neurosci 33:16297-16309.
750 Guerrieri F, Schubert M, Sandoz JC, Giurfa M (2005) Perceptual and neural olfactory
751 similarity in honeybees. PLoS Biol 3:e60.
752 Hallem EA, Carlson JR (2006) Coding of odors by a receptor repertoire. Cell
753 125:143-160.
754 Haverkamp S, Wässle H, Duebel J, Kuner T, Augustine GJ, Feng G, Euler T (2005)
755 The Primordial, Blue-Cone Color System of the Mouse Retina. J Neurosci
756 25:5438-5445.
757 Hong Elizabeth J, Wilson Rachel I (2015) Simultaneous Encoding of Odors by
758 Channels with Diverse Sensitivity to Inhibition. Neuron 85:573-589.
759 Knaden M, Strutz A, Ahsan J, Sachse S, Hansson BS (2012) Spatial Representation
760 of Odorant Valence in an Insect Brain. Cell Reports 1:392-399.
761 Kuner T, Augustine GJ (2000) A Genetically Encoded Ratiometric Indicator for
762 Chloride: Capturing Chloride Transients in Cultured Hippocampal Neurons.
763 Neuron 27:447-459.
764 Kurahashi T, Yau KW (1993) Co-existence of cationic and chloride components in
765 odorant-induced current of vertebrate olfactory receptor cells. Nature 363:71-
766 74.
767 Labarrera C, London M, Angelo K (2013) Tonic inhibition sets the state of excitability
768 in olfactory bulb granule cells. The Journal of Physiology 591:1841-1850.

769 Laissue PP, Reiter C, Hiesinger PR, Halter S, Fischbach KF, Stocker RF (1999)
770 Three-dimensional reconstruction of the antennal lobe in *Drosophila*
771 *melanogaster*. J Comp Neurol 405:543-552.
772 Laurent G, Stopfer M, Friedrich RW, Rabinovich MI, Volkovskii A, Abarbanel HDI
773 (2001) Odor encoding as an active, dynamical process: Experiments,
774 computation and theory. Annu Rev Neurosci 24:263-297.
775 Liu WW, Wilson RI (2013) Glutamate is an inhibitory neurotransmitter in the
776 Drosophila olfactory system. Proc Natl Acad Sci 110:10294-10299.
777 Lowe G, Gold GH (1993) Nonlinear amplification by calcium-dependent chloride
778 channels in olfactory receptor cells. Nature 366:283-286.
779 Margrie TW, Schaefer AT (2003) Theta oscillation coupled spike latencies yield
780 computational vigour in a mammalian sensory system. The Journal of
781 Physiology 546:363-374.
782 Martelli C, Fiala A (2019) Slow presynaptic mechanisms that mediate adaptation in
783 the olfactory pathway of Drosophila. eLife 8:e43735.
784 Messina A, Neri M, Perosa F, Caggese C, Marino M, Caizzi R, De Pinto V (1996)
785 Cloning and chromosomal localization of a cDNA encoding a mitochondrial
786 porin from Drosophila melanogaster. FEBS Letters 384:9-13.
787 Miyawaki A, Griesbeck O, Heim R, Tsien RY (1999) Dynamic and quantitative Ca2+
788 measurements using improved cameleons. Proc Natl Acad Sci 96:2135-2140.
789 Mohamed AAM, Retzke T, Das Chakraborty S, Fabian B, Hansson BS, Knaden M,
790 Sachse S (2019) Odor mixtures of opposing valence unveil inter-glomerular
791 crosstalk in the Drosophila antennal lobe. Nature Communications 10:1201.
792 Mori K, Nagao H, Yoshihara Y (1999) The olfactory bulb: coding and processing of
793 odor molecule information. Science 286:711-715.
794 Nagel KI, Hong EJ, Wilson RI (2014) Synaptic and circuit mechanisms promoting
795 broadband transmission of olfactory stimulus dynamics. Nat Neurosci 18:56.
796 Niewalda T, Völler T, Eschbach C, Ehmer J, Chou W-C, Timme M, Fiala A, Gerber B
797 (2011) A Combined Perceptual, Physico-Chemical, and Imaging Approach to
798 'Odour-Distances' Suggests a Categorizing Function of the Drosophila
799 Antennal Lobe. PLoS ONE 6:e24300.
800 O'Donnell MJ, Rheault MR, Davies SA, Rosay P, Harvey BJ, Maddrell SHP, Kaiser
801 K, Dow JAT (1998) Hormonally controlled chloride movement across
802 Drosophila tubules is via ion channels in stellate cells. American Journal of
803 Physiology-Regulatory, Integrative and Comparative Physiology 274:R1039-
804 R1049.
805 Olsen SR, Wilson RI (2008) Lateral presynaptic inhibition mediates gain control in an
806 olfactory circuit. Nature 452:956-960.
807 Owens DF, Kriegstein AR (2002) Is there more to gaba than synaptic inhibition? Nat
808 Rev Neurosci 3:715-727.
809 Pelz D, Roeske T, Syed Z, Bruyne Md, Galizia CG (2006) The molecular receptive
810 range of an olfactory receptor in vivo (Drosophila melanogaster Or22a). J
811 Neurobiol 66:1544-1563.
812 Pézier A, Grauso M, Acquistapace A, Monsempes C, Rospars J-P, Lucas P (2010)
813 Calcium Activates a Chloride Conductance Likely Involved in Olfactory
814 Receptor Neuron Repolarization in the Moth Spodoptera littoralis. J Neurosci
815 30:6323-6333.
816 Reinert A, Barapatre N, Sachse S, Reinert T (2011) μPIXE for a μBrain: The vinegar
817 fly's brain, antenna, sensilla hairs and eye ion concentrations. Nuclear
818 Instruments and Methods in Physics Research Section B 269:2292-2296.

819 Riemensperger T, Pech U, Dipt S, Fiala A (2012) Optical calcium imaging in the
820 nervous system of Drosophila melanogaster. Biochimica et Biophysica Acta
821 (BBA) - General Subjects 1820:1169-1178.
822 Root CM, Masuyama K, Green DS, Enell LE, Nässel DR, Lee C-H, Wang JW (2008)
823 A Presynaptic Gain Control Mechanism Fine-Tunes Olfactory Behavior.
824 Neuron 59:311-321.
825 Rytz R, Croset V, Benton R (2013) Ionotropic Receptors (IRs): Chemosensory
826 ionotropic glutamate receptors in Drosophila and beyond. Insect Biochemistry
827 and Molecular Biology 43:888-897.
828 Sachse S, Galizia CG (2002) Role of inhibition for temporal and spatial odor
829 representation in olfactory output neurons: a calcium imaging study. J
830 Neurophysiol 87:1106-1117.
831 Sachse S, Galizia CG (2003) The coding of odour-intensity in the honeybee antennal
832 lobe: local computation optimizes odour representation. Eur J Neurosci
833 18:2119-2132.
834 Sato K, Pellegrino M, Nakagawa T, Nakagawa T, Vosshall LB, Touhara K (2008)
835 Insect olfactory receptors are heteromeric ligand-gated ion channels. Nature
836 452:1002.
837 Schoppa NE, Westbrook GL (1999) Regulation of synaptic timing in the olfactory
838 bulb by an A-type potassium current. Nat Neurosci 2:1106-1113.
839 Schoppa NE, Urban NN (2003) Dendritic processing within olfactory bulb circuits.
840 Trends Neurosci 26:501-506.
841 Schubert M, Hansson BS, Sachse S (2014) The banana code – Natural blend
842 processing in the olfactory circuitry of Drosophila melanogaster. Frontiers in
843 Physiology 5.
844 Seki Y, Rybak J, Wicher D, Sachse S, Hansson BS (2010) Physiological and
845 Morphological Characterization of Local Interneurons in the Drosophila
846 Antennal Lobe. J Neurophysiol 104:1007-1019.
847 Seki Y, Dweck HKM, Rybak J, Wicher D, Sachse S, Hansson BS (2017) Olfactory
848 coding from the periphery to higher brain centers in the Drosophila brain.
849 BMC Biology 15:56.
850 Shanbhag SR, Muller B, Steinbrecht RA (1999) Atlas of olfactory organs of
851 *Drosophila melanogaster*. 1. Types, external organization, innervation and
852 distribution of olfactory sensilla. Int J Insect Morphol Embryol 28:377-397.
853 Silbering AF, Galizia CG (2007) Processing of Odor Mixtures in the Drosophila
854 Antennal Lobe Reveals both Global Inhibition and Glomerulus-Specific
855 Interactions. J Neurosci 27:11966-11977.
856 Staley KJ, Proctor WR (1999) Modulation of mammalian dendritic GABAA receptor
857 function by the kinetics of Cl− and HCO3− transport. The Journal of
858 Physiology 519:693-712.
859 Steinbrecht RA (1992) Experimental morphology of insect olfaction: Tracer studies,
860 x-ray microanalysis, autoradiography, and immunocytochemistry with silkmoth
861 antennae. Micros Res Tech 22:336-350.
862 Stephan AB, Shum EY, Hirsh S, Cygnar KD, Reisert J, Zhao H (2009) ANO2 is the
863 cilial calcium-activated chloride channel that may mediate olfactory
864 amplification. Proc Natl Acad Sci 106:11776-11781.
865 Stocker RF, Heimbeck G, Gendre N, de Belle JS (1997) Neuroblast ablation in
866 *Drosophila* P[GAL4] lines reveals origins of olfactory interneurons. J Neurobiol
867 32:443-456.

868 Stopfer M, Bhagavan S, Smith BH, Laurent G (1997) Impaired odour discrimination
869 on desynchronization of odour-encoding neural assemblies. Nature 390:70-74.
870 Strutz A, Voeller T, Riemensperger T, Fiala A, Sachse S (2012) Calcium Imaging of
871 Neural Activity in the Olfactory System of *Drosophila*. In: Genetically Encoded
872 Functional Indicators (Martin J-R, ed), pp 43-70. New York, NY, USA:
873 Springer Science+Business Media, LLC.
874 Tian L, Hires SA, Mao T, Huber D, Chiappe ME, Chalasani SH, Petreanu L,
875 Akerboom J, McKinney SA, Schreiter ER, Bargmann CI, Jayaraman V,
876 Svoboda K, Looger LL (2009) Imaging neural activity in worms, flies and mice
877 with improved GCaMP calcium indicators. Nat Meth 6:875-881.
878 Urban NN (2002) Lateral inhibition in the olfactory bulb and in olfaction. Physiol
879 Behav 77:607-612.
880 Vosshall LB, Wong AM, Axel R (2000) An olfactory sensory map in the fly brain. Cell
881 102:147-159.
882 Wang JW, Wong AM, Flores J, Vosshall LB, Axel R (2003) Two-photon calcium
883 imaging reveals an odor-evoked map of activity in the fly brain. Cell 112:271-
884 282.
885 Wicher D, Walther C, Wicher C (2001) Non-synaptic ion channels in insects — basic
886 properties of currents and their modulation in neurons and skeletal muscles.
887 Prog Neurobiol 64:431-525.
888 Wicher D, Schafer R, Bauernfeind R, Stensmyr MC, Heller R, Heinemann SH,
889 Hansson BS (2008) Drosophila odorant receptors are both ligand-gated and
890 cyclic-nucleotide-activated cation channels. Nature 452:1007-1011.
891 Wilson RI, Laurent G (2005) Role of GABAergic inhibition in shaping odor-evoked
892 spatiotemporal patterns in the *Drosophila* antennal lobe. J Neurosci 25:9069-
893 9079.
894 Wilson RI, Mainen ZF (2006) Early events in olfactory processing. Annu Rev
895 Neurosci 29:163-201.
896 Wilson RI, Turner GC, Laurent G (2004) Transformation of olfactory representations
897 in the *Drosophila* antennal lobe. Science 303:366-370.
898 Zhu P, Frank T, Friedrich RW (2013) Equalization of odor representations by a
899 network of electrically coupled inhibitory interneurons. Nat Neurosci 16:1678.
900
901

902 **Figure Legends**

903 **Figure 1. Clomeleon is a functional chloride indicator in *Drosophila* olfactory**
904 **neurons.**

905 ***A, B,*** Schematic of AL neurons indicating expression site of Clomeleon with images
906 of brain preparation showing Clomeleon YFP baseline fluorescence (***A***: olfactory
907 sensory neurons, OSNs; ***B***: projection neurons, PNs). AL, antennal lobe; CX, calyx;
908 LP, lateral protocerebrum. ***C, D,*** Fluorescence change in a representative animal
909 over time of CFP, YFP and YFP:CFP ratio induced by potassium gluconate
910 application (KGlu, 1M, 20 µl) into saline (300 µl) in OSNs (***C***) and PNs (***D***). ***E, F,***
911 Time course of $[Cl^-]_i$ increase induced by applying KGlu (arrowhead) averaged
912 across several animals in OSNs (E) and PNs (F). Color shading indicates standard
913 deviation, n=6-10. ***G, H,*** Time courses of $[Cl^-]_i$ increase induced by GABA application
914 (1M, 20 µl) into saline (300 µl) averaged across several animals in OSNs (***G***) and
915 PNs (***H***). Insets show enlarged area around the time point of GABA application.
916 Dashed lines mark the biphasic response threshold. Color shading indicates
917 standard deviation, n=6-9. ***I,*** Effect of Cl^- free saline application on Cl^- changes
918 evoked by ethyl-3-hydroxybutyrate in OSNs. Box plots represent median value
919 (horizontal line inside the box), interquartile range (box) and minimum/maximum
920 value (whiskers). Removing Cl^- significantly reduced the Clomeleon signal
921 (***$p<0.001$, repeated measures ANOVA, n=13). ***J,*** Effect of chloride channel
922 blocker NPPB (500 µM) application on Cl^- signals evoked by ethyl-3-hydroxybutyrate
923 in OSNs (**$p<0.01$, *$p<0.05$, repeated measures ANOVA, n=7). ***K,*** Quantification of
924 Clomeleon baseline fluorescence in OSNs at different saline pH in relation to
925 standard condition (i.e. pH=7.3). Arrangement of different box plots from left to right

926 reflects temporal sequence of the experiment (p= 0.144, repeated measures ANOVA,
927 n=11).
928
929 **Figure 2. Odor application induces spatially confined chloride influx in**
930 **olfactory sensory neurons in the *Drosophila* antenna.**
931 ***A,*** Network model scheme of neuronal connectivity in the fly AL. ***B,*** Clomeleon YFP
932 baseline fluorescence in OSN dendrites in the *Drosophila* antenna (Ant).
933 ***C,*** Schematic of olfactory sensilla distribution on the third antennal segment. Sensilla
934 marked in green are labeled by *Orco-Gal4*. ***D,*** Pseudocolor rendering of odor-evoked
935 changes in Cl^- concentration using Clomeleon (upper row) and in Ca^{2+} concentration
936 using Cameleon (lower row) in response to different odors and mineral oil in OSN in
937 the antenna. Images represent $\Delta R/R$ (%) superimposed onto raw fluorescence
938 images according to the scales and color codes on the right. Time courses on the
939 right reveal representative Cl^- and Ca^{2+} signals for different odors across the entire
940 antennal segment. Odor application is indicated by a grey bar. ***E,*** Quantification of
941 Cl^- (left) and Ca^{2+} (right) responses to different odors and mineral oil (n.s., not
942 significant from solvent; repeated measures ANOVA followed by Dunnett Multiple
943 Comparisons Test, n=8). ***F,*** Maximum intensity projection of Clomeleon expressed in
944 the antenna under the control of *Or47b-Gal4*. Time courses of normalized Cl^-
945 responses to the solvent control mineral oil and ethyl-3-hydroxybutyrate (n=8). ***G,***
946 Schematic of the connection between the antenna and AL via the antennal nerve
947 (AN), which was disrupted here. Time course of normalized Cl^- responses to ethyl-3-
948 hydroxybutyrate in 3 animals of the left antenna (AN intact, solid line) and right
949 antenna after the right antennal nerve was cut (AN cut, dotted line). Lines indicate
950 means, color shading gives SEM (*$p < 0.05$, two-way ANOVA).

951

952 **Figure 3. An odor-specific spatial map of chloride responses in antennal lobe**
953 **sensory neurons.**

954 ***A,*** Schematic illustrating the expression site of Clomeleon (AL, antennal lobe; AN,
955 antennal nerve; CX, calyx; LP, lateral protocerebrum). ***B,*** Left, Clomeleon YFP
956 baseline fluorescence in axon termini of OSNs in the AL with anatomical
957 identification of individual glomeruli. Right, schematic AL map viewed from the angle
958 used for imaging experiments. Glomeruli marked in orange could reliably be
959 identified. AC, antennal commissure. ***C,*** Pseudocolor rendering of Cl^- responses to
960 different odors and mineral oil in OSN axon termini in the AL of two different
961 individuals. Images represent $\Delta R/R$ (%) superimposed onto raw fluorescence images
962 according to the scales on the right. Numbers in each image represent individual
963 fluorescence minimum. Glomerular positions are shown in the first image; glomeruli
964 revealing highest Cl^- increase are indicated in each image. The minimum of the
965 scaling is indicated in each frame in the upper right corner. ***D,*** Time courses of Cl^-
966 influx for each odor and mineral oil averaged across 6-9 animals. Individual glomeruli
967 are indicated by different colors, odor stimulation is marked in grey. ***E,*** False color
968 pictures of averaged odor-evoked Cl^- signals for 14 glomeruli (42% of all glomeruli
969 labeled by *Orco-Gal4*) over time across 6-9 animals. Clomeleon responses were
970 normalized to highest Cl^- influx in each animal over all odors before averaging. Black
971 bar indicates odor application. ***F-H,*** Representative time courses of Cl^- influx to
972 repeated stimulations of ethyl-3-hydroxybutyrate using interstimulus intervals of 10 s
973 (***F***), 60 s (***G***) or 120 s (***H***). Odor stimulations are marked in grey.

974

975 **Figure 4. Chloride responses are modulated on their way from the antenna to**
976 **the antennal lobe.**
977 ***A,*** Left, schematic of the third antennal segment illustrating selective expression of
978 Cameleon or Clomeleon in dendrites and somata of Or22a-expressing OSNs. Right,
979 averaged time courses of Ca^{2+} (upper row) and Cl^- influx (lower row) in Or22a-
980 expressing OSNs in the fly antenna to 3 different odors. Odor stimulation is indicated
981 in grey. Lines represent means, color shadings represent SEM (n=6-7). ***B,*** Left,
982 schematic of the *Drosophila* AL indicating selective expression of Cameleon or
983 Clomeleon in axonal termini of Or22a-expressing OSNs which converge to
984 glomerulus DM2. Right, averaged time courses of Ca^{2+} (upper row) and Cl^- influx
985 (lower row) in DM2 to 3 different odors. Odor stimulation is marked in grey. Lines
986 represent means, color shading represents SEM (n=6). ***C,D,*** Quantification of Ca^{2+}
987 (***C***) and Cl^- (***D***) influx in Or22a-expressing OSNs to 3 different odors and mineral oil.
988 Data are shown as pair-wise comparisons between antenna (Or22a) and AL (DM2).
989 Clomeleon and Cameleon responses have been normalized to highest Cl^- or Ca^{2+}
990 influx in each animal over all odors, respectively. Cl^- responses to ethyl-3-
991 hydoxybutyrate and benzaldehyde are significantly lower in the AL compared to the
992 antenna (** $p<0.01$, *** $p<0.001$, Mann-Whitney test, n=6-7).
993
994 **Figure 5. $GABA_A$ receptors contribute to odor-evoked chloride responses in**
995 **projection neurons.**
996 ***A,*** Left, schematic illustrating expression site of Clomeleon. Middle, AL map viewed
997 from the angle that was used for imaging. Glomeruli indicated in green could reliably
998 be identified. Right, contra lateral AL including reliably identified glomeruli. APT,
999 antenno-protocerebral tract. ***B,*** Pseudocolor rendering of representative Cl^-

1000 responses to different odors and mineral oil in PN dendrites in the AL. Images
1001 represent ΔR/R (%) superimposed onto raw fluorescence images according to the
1002 scale on the right. Numbers in each image give the individual fluorescence minimum.
1003 Glomerular positions are shown in the first image; individual glomeruli revealing
1004 highest Cl^- increase are indicated in each image. ***C,*** False color pictures of averaged
1005 odor-evoked Cl^- signals for 12 identified glomeruli (40% of all glomeruli labeled by
1006 *GH146-Gal4*) over time across 9-11 animals. Clomeleon responses were normalized
1007 to highest Cl^- influx in each animal over all odors before averaging. Black bar
1008 indicates the odor application. ***D,*** Quantification of Cl^- influx to ethyl-3-
1009 hydroxybutyrate in PNs before, during and after applying of picrotoxin. The $GABA_A$
1010 receptor blocker significantly reduces odor-evoked Cl^- responses (**$p<0.01$, repeated
1011 measures ANOVA, n=9).
1012
1013 **Figure 6. A functional map of odor-evoked inhibition and excitation.**
1014 ***A,B,*** Averaged odor-evoked Cl^- (left, in blue) and Ca^{2+} (right, in red) responses in
1015 OSNs (***A***) and PNs (***B***) are represented as schematic ALs for 11 odors according to
1016 the scales below. Responses were normalized to highest Cl^- or Ca^{2+} influx in each
1017 animal over all odors. Glomerular identities are indicated by AL maps at the top. AC,
1018 antennal commissure; AN, antennal nerve; ALT, antennal lobe tract.
1019
1020 **Figure 7. Input-output transformation of odor-evoked Ca^{2+} and Cl^- responses.**
1021 ***A,*** False colored activity of averaged odor-evoked Ca^{2+} (white-yellow-red) and Cl^-
1022 (white-green-blue) influx to different odors for the same set of glomeruli in OSNs
1023 (upper panels) and PNs (lower panels) over time. Responses were normalized to
1024 highest Cl^- or Ca^{2+} influx in each animal over all odors before averaging. Black bars

1025 indicate odor application. ***B,*** Time courses of mean excitation (above, red) and
1026 inhibition (below, blue) to different odors averaged over all glomeruli and animals for
1027 OSNs (solid line) and PNs (dotted line). Odor stimulation is given by a grey bar.
1028 Cameleon, n=7; Clomeleon, n=9-11. ***C,*** Odor separation visualized using principal
1029 component analysis. Plotting the first three principal components reveals odor
1030 specific trajectories of ensemble activity in OSNs (upper panels) and PNs (lower
1031 panels). ***D,*** *Upper two panels*, time-resolved Euclidean distances between population
1032 vectors of different odor representations using Cameleon. Odor stimulation is
1033 marked in grey. Distances were calculated separately for OSN (solid lines) and PN
1034 (dotted lines) responses. Individual pair-wise odor distances are given by thin lines,
1035 averaged Euclidean distances are shown in bold. *Lower panel*, latency to half
1036 maximal odor separation based on normalized Euclidean distances for 10 pair-wise
1037 odor combinations (individual lines in ***B***) for Ca^{2+} signals in OSNs and PNs. PNs
1038 reach half maximum odor separation significantly earlier than OSNs (***$p<0.001$,
1039 two-tailed paired t-test; n=7). ***E***, Same as in ***D*** for Clomeleon-derived odor responses.
1040 Half maximum odor separation based on odor-evoked Cl^- responses occurs
1041 significantly earlier in PNs than in OSNs (*$p<0.05$, two-tailed paired t-test; n=9-11).

Figure 1

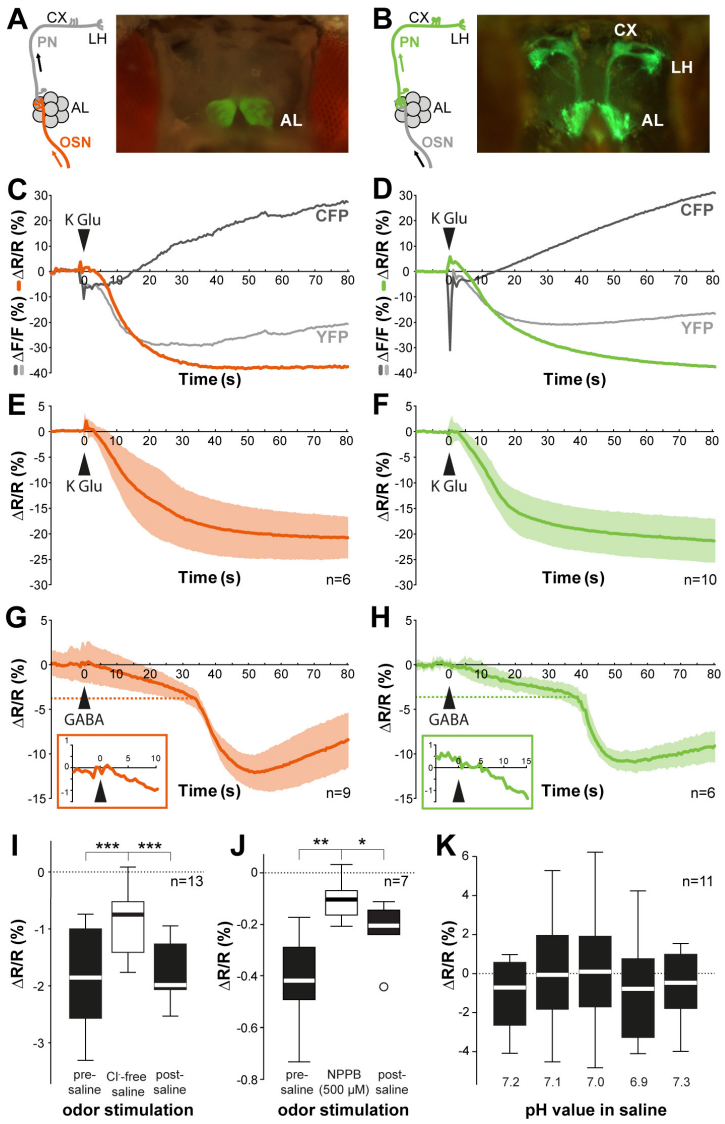

Figure 2

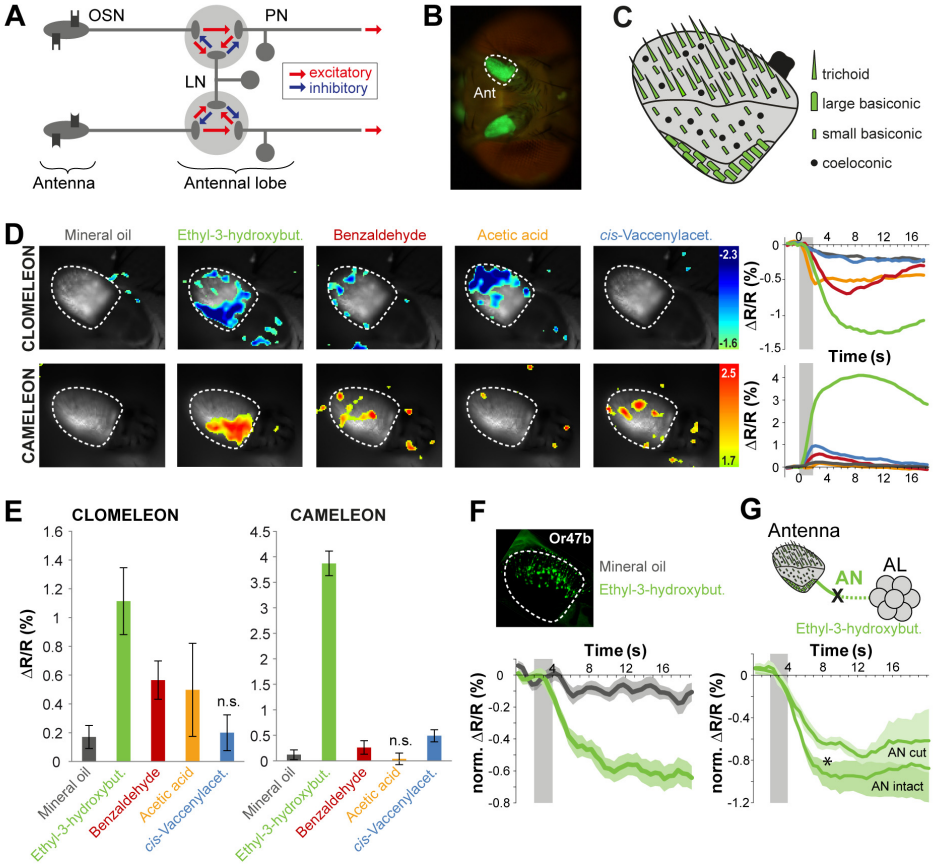

Figure 3

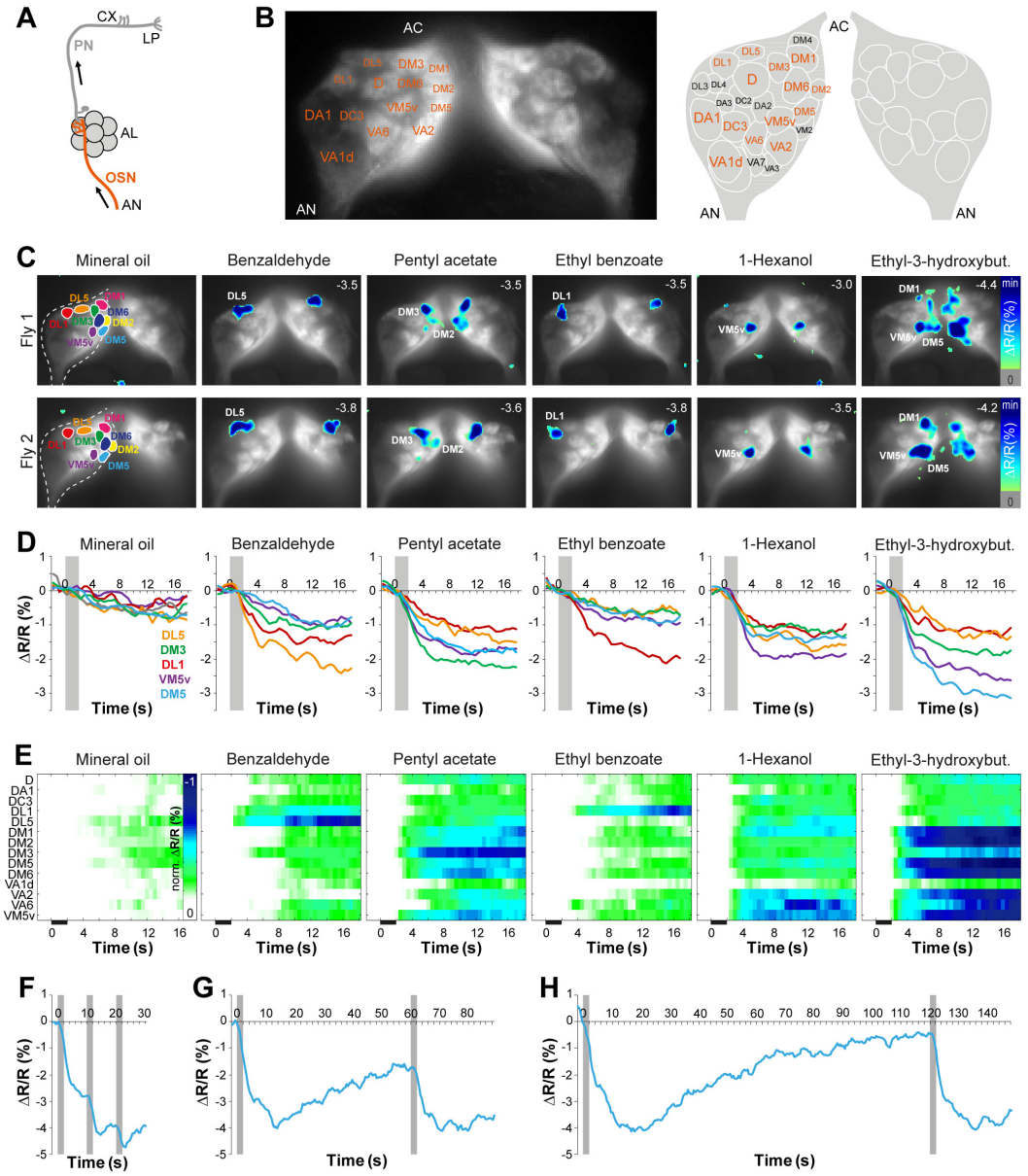

Figure 4

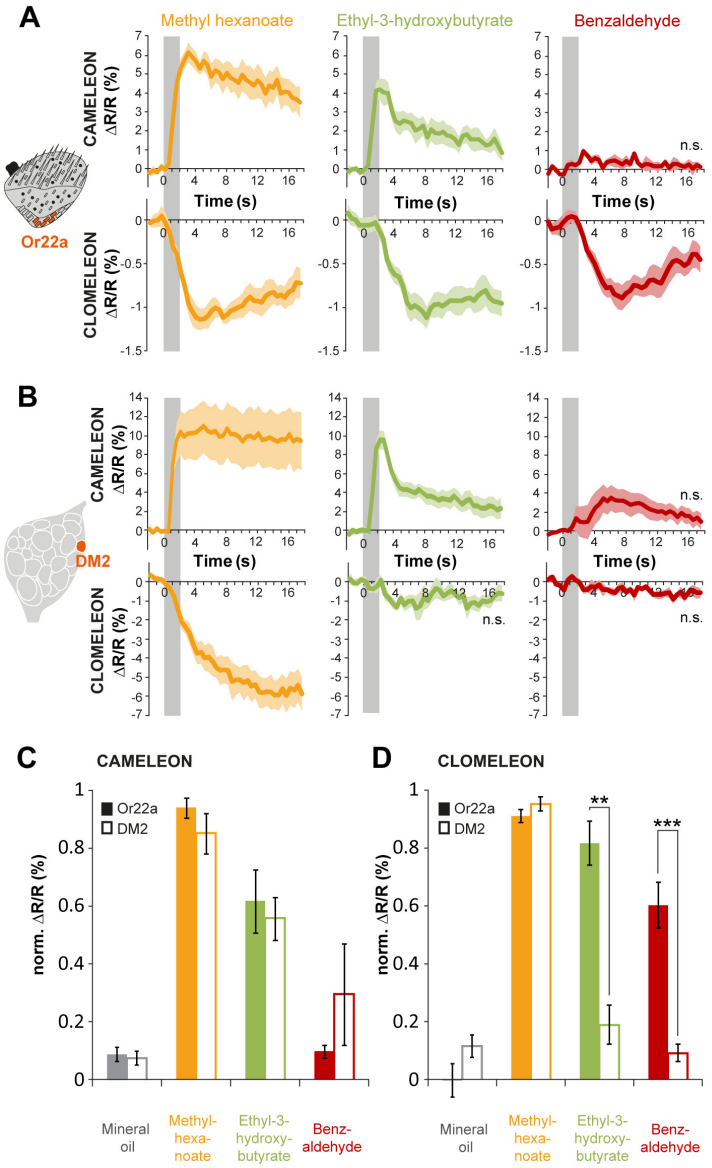

Figure 5

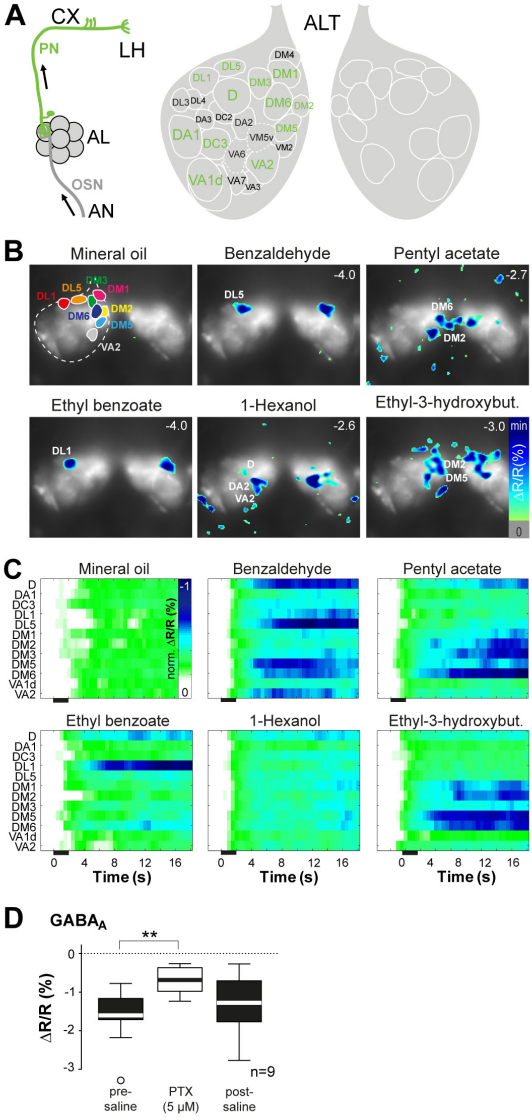

Figure 6

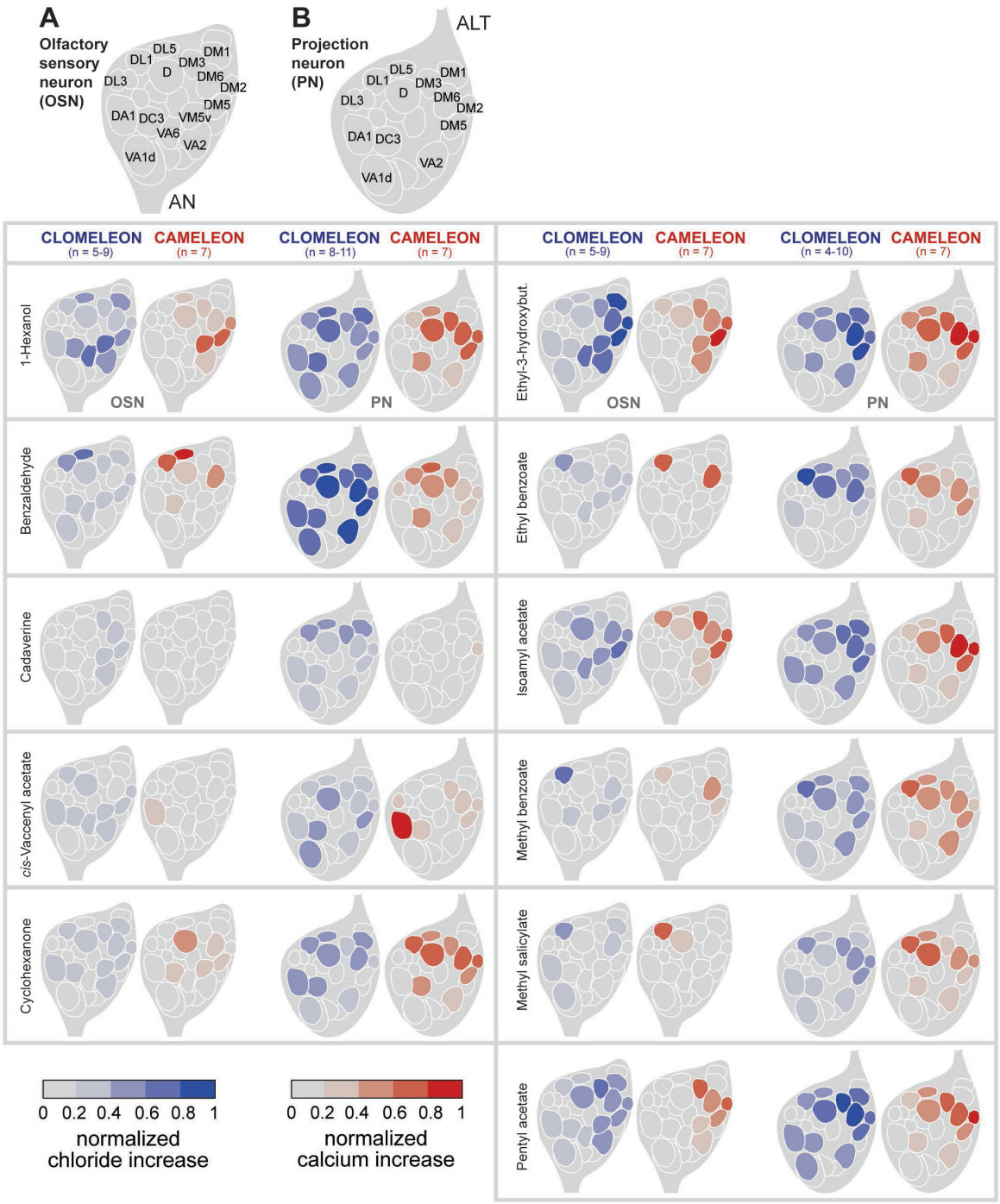

Figure 7